Semiclassical analysis of a detuned ring laser with a saturable absorber: New results for the steady states

D. E. Chyba,* N. B. Abraham, and A. M. Albano
Department of Physics, Bryn Mawr College, Bryn Mawr, Pennsylvania 19010
(Received 29 August 1986)

This paper presents new results for the steady states of a detuned ring laser with a saturable absorber. We employ a semiclassical model which assumes homogeneously broadened two-level atoms. We proceed by solving the Maxwell-Bloch equations for the longitudinal dependence of the steady states of this system, and then simplify our solution by use of the uniform-field approximation. We present uniform-field results for squared electric field versus operating frequency, and for each of these versus cavity tuning and laser excitation. Various cavity linewidths and both resonant and nonresonant amplifier and absorber line-center frequencies are considered. The most notable finding is that cavity detuning breaks the degeneracies found in the steady-state solutions of the fully tuned case. This leads to the prediction that an actual system will bifurcate from the zero-intensity solution to a steady-state solution as laser excitation increases from zero, rather than to the small-amplitude pulsations found for the model with exactly resonant tuning of the cavity and the media line centers. Other phenomena suggested by the steady-state results include tuning-dependent hysteresis and bistability, and instability in both intensity and frequency due to the appearance of one or more new steady-state solutions as tuning is varied. These effects of detuning are being tested by a linearized stability analysis whose results will be reported separately.

I. INTRODUCTION

In this paper we present new theoretical results for the steady states of homogeneously broadened, detuned ring laser with a saturable absorber. This work is part of a general study of the time-dependent and time-independent solutions of this system. The results given here represent a step forward in our ability to incorporate cavity detuning into the treatment of this system and to allow different resonant frequencies for the absorbing and amplifying atoms. We will present results on the stability of the steady-state solutions in a later paper.

Recent theoretical investigations of instabilities, bifurcations, and dynamical behavior in this system have so far been restricted to the "fully tuned" case, in which the resonant frequencies of the amplifying and absorbing atoms are equal and match the cavity tuning (for example, Refs. 1—4). We are able to lift both of these restrictions, and can therefore examine the dependence of the possible steady-state solutions on the cavity tuning, and on the frequency mismatch between the amplifying and absorbing atoms. We have found that detuning the cavity removes degeneracies otherwise present in the steady-state solutions,[2(a)—2(d)] suggesting that there may also be interesting departures from the stability behavior found in the fully tuned case.[1—4] Similar effects of detuning on the steady-state solutions for a model of the far-infrared laser have been found by Wu and Mandel.[5]

An additional feature of our method is the ability to compute the longitudinal dependences of the state variables describing the system, and thereby to allow for nonsaturable losses.[6] In the present paper we derive the full solutions with longitudinal dependence, simulating arbitrary nonsaturable losses by assuming mirrors of arbitrary reflectivity. In order to simplify our initial calculations and to compare our results with those of other workers, we then apply the uniform-field approximation of Bonifacio and Lugiato.[7(a)] This approximation, which removes the longitudinal dependence, has been used throughout the studies of Refs. 1—4. On the other hand, Arimondo and Dinelli modified the model used in Refs. 1—4 in order to take account of the significant losses actually encountered in their experimental system.[8] Thus solutions containing the effects of the longitudinal variations in the field necessitated by nonsaturable losses are eventually of interest. An examination of the results given by our model without the uniform-field approximation will be presented elsewhere.

Our model for the ring laser with a saturable absorber entails the following simplifications: atoms of both types are modeled as two-level atoms experiencing only homogeneous broadening of their spectral lines. The two media are taken to be uniformly mixed in a single cell, but are assumed to interact only through the electric field. We model this system by the semiclassical Maxwell-Bloch equations, and assume the existence of single-frequency solutions in the slowly-varying-amplitude approximation. We also assume unidirectional propagation of light around the ring. Polarization of the light, and radial variation of the state variables of the system with respect to the optical axis, are not considered.

The model so extensively developed in Refs. 1—4 also assumes homogeneously broadened two-level atoms and the existence of single-frequency solutions. A variety of other approaches to the problem of the laser with a saturable absorber, which remove one or more of these restrictions, are given in Refs. 9—15. However, most of these studies have employed the simpler rate-equation approxi-

mation, and many, though not all, treat only the fully tuned case. We have found the model described above to be a good starting point for a more complete treatment of the effects of adjusting the cavity tuning and the atomic line-center frequencies of the two media. A review of laser instabilities, including theoretical work on the homogeneously broadened two-level atom model for a laser with a saturable absorber, is being prepared by Abraham, Mandel, and Narducci.[16]

Lasers with intracavity saturable absorbers have been of experimental interest for many years in such applications as spectroscopy,[15,17] frequency stabilization,[18] and mode locking, self-pulsing, and pulse shaping.[19] Careful experimental studies of the dynamical behavior of these systems have now been undertaken by a number of workers.[8,13,20–22] Bistability[8,21] and Q switching[13,20,22] have been particularly studied. This exciting work has stimulated the further development of theoretical models[8,13] in addition to testing the dynamical predictions of the theorists.[20(c),20(d)] The theoretical and experimental study of bistability reported in Ref. 8 was concerned with the fully tuned case. Similarly, the detailed studies of Q switching reported in Refs. 13 and 20 used resonant rate equations to model the media as four-level systems. An expanded theory of passive Q switching which incorporates dispersion is needed for the interpretation of data on the effects of cavity tuning.[20(c)]

We have organized the paper as follows. In Sec. II we derive the steady-state solutions as implicit functions with full dependence on longitudinal position and all the parameters of our model. In Sec. III we apply the uniform-field approximation to these solutions. We then cast the results of this procedure into a form analogous to that obtained by Casperson and Yariv in their study of the multiple operating points of an inhomogeneously broadened laser.[23] This results in a particularly physical picture of the steady-state solutions and their dependence on the parameters of the system.

However, the equations themselves are still quite complicated. In Secs. IV–VI we assume physically interesting values for the model parameters and perform numerical calculations in order to visualize our results. In Secs. IV and V, we assume that the amplifying and absorbing atoms have the same line-center frequency. In Sec. IV we obtain plots illustrating the relationships between the state variables of the system and the operating frequency. We then use these relationships to find the parameter dependences of the solutions for the operating frequency and for the squared modulus of the electric field. The adjustable parameters we consider are cavity detuning, cavity linewidth, and excitation of the amplifying medium. The results of variations in these parameters are discussed in detail in Sec. V. In Sec. VI we undertake a similar analysis assuming unequal line-center frequencies for the two media. Section VII is a summary and conclusion.

II. THEORETICAL APPROACH AND STEADY-STATE SOLUTIONS WITH FULL LONGITUDINAL DEPENDENCE

We have been especially influenced in our approach to this problem by the methods of Casperson and Yariv[23] and of Lugiato, Mandel, and their co-workers.[1,2,7] Our initial Maxwell-Bloch equations correspond to the semiclassical equations derived by the latter authors, but allow longitudinal variation of the electric field, detuning of the cavity, and unequal line-center frequencies for the gain and loss media. Figure 1 shows a schematic diagram of the ring system. The Maxwell-Bloch Equations for this problem are then the following:

$$\frac{\partial E}{\partial t}=-c\frac{\partial E}{\partial z}-g_a S_a-g_b S_b\ , \tag{2.1a}$$

$$\frac{\partial S_a}{\partial t}=-(\gamma_{\perp a}+i\Delta\omega_a)S_a+\frac{\mu_a}{\hbar}ED_a\ , \tag{2.1b}$$

$$\frac{\partial S_b}{\partial t}=-(\gamma_{\perp b}+i\Delta\omega_b)S_b+\frac{\mu_b}{\hbar}ED_b\ , \tag{2.1c}$$

$$\frac{\partial D_a}{\partial t}=-\gamma_{\parallel a}\left[D_a+\frac{N_a}{2}\right]-\frac{\mu_a}{2\hbar}(ES_a^*+E^*S_a)\ , \tag{2.1d}$$

$$\frac{\partial D_b}{\partial t}=-\gamma_{\parallel b}\left[D_b-\frac{N_b}{2}\right]-\frac{\mu_b}{2\hbar}(ES_b^*+E^*S_b)\ . \tag{2.1e}$$

These equations must be supplemented by the ring-cavity boundary condition[24]

$$E(0,t)=E(L,t-\Delta t)R\exp(-i\Delta\omega_c t_R)\ . \tag{2.2}$$

The symbols used in these equations are defined as follows. The "state variables" E, S, and D are, respectively, the slowly varying amplitudes of the electric field, the electric polarization of the medium, and the "population difference" for the medium. The subscripts a and b refer to the amplifying and absorbing media, respectively. These are all functions of longitudinal position z (along the optical axis of the cavity) and time t, with propagation of light occurring in the positive z direction. Population difference, as usual, means $\frac{1}{2}(N_1-N_2)$ for each medium, where N_1 and N_2 are the populations of the lower and upper levels. g_a and g_b are the polarization-field coupling constants; $g_a=4\pi\omega_0\mu_a/V$ and $g_b=4\pi\omega_0\mu_b/V$. Here ω_0 is the angular frequency of the light field, μ_a and μ_b are the electric dipole transition moments for the two media, and V is the volume of the mixed media through which

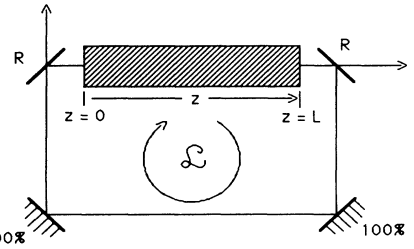

FIG. 1. Schematic diagram of the model ring laser with a saturable absorber. The ring cavity of total length $\mathscr{L}$ is defined by four mirrors, of which two are 100% reflecting and two have reflectivity $R<1$. The spatial coordinate z measures position along the medium cell in the direction of propagation of the light. The cell has length L and contains a homogeneous mixture of absorbing and amplifying media.

the beam passes. $\gamma_{\perp a}$, $\gamma_{\perp b}$ are spontaneous decay rates for the electrical polarizations of the media, and $\gamma_{\|a}$, $\gamma_{\|b}$ are the corresponding rates for the population differences for media a and b.

$\Delta\omega_a$, $\Delta\omega_b$, and $\Delta\omega_c$ are defined by

$$\begin{aligned}\Delta\omega_a &= \omega_a - \omega_0 ,\\ \Delta\omega_b &= \omega_b - \omega_0 ,\\ \Delta\omega_c &= \omega_c - \omega_0 ,\end{aligned} \tag{2.3}$$

where ω_a and ω_b are the angular frequencies at line center for the amplifying and absorbing media, and ω_c is the angular frequency of the empty-cavity mode nearest to the laser operating frequency ω_0. For a ring cavity of round-trip length $\mathscr{L}$, this mode may be characterized by the (empty-cavity) wavelength λ_c and the integral mode number $m_c = \mathscr{L}/\lambda_c$, such that $\omega_c = 2\pi m_c c/\mathscr{L}$. For purposes of computation, it will later be convenient to refer each of the ω's and $\Delta\omega$'s to the frequency ω_a by introducing the relative frequencies

$$\Delta\omega_0 = \omega_0 - \omega_a , \tag{2.4a}$$

$$\Delta\omega_{ab} = \omega_b - \omega_a , \tag{2.4b}$$

$$\Delta\omega_{ac} = \omega_c - \omega_a , \tag{2.4c}$$

so that

$$\begin{aligned}\Delta\omega_a &= -\Delta\omega_0 ,\\ \Delta\omega_b &= \Delta\omega_{ab} - \Delta\omega_0 ,\\ \Delta\omega_c &= \Delta\omega_{ac} - \Delta\omega_0 .\end{aligned} \tag{2.5}$$

We will refer to $\Delta\omega_{ac}$ as the "cavity detuning" (relative to the amplifying atom line center), in analogy to the common designation of ω_c as the "cavity tuning".

N_a and N_b are the numbers of active a and b atoms in the effective volume V, and thus represent the excitation of the media, or "pumping." As indicated in Fig. 1, the cell containing the media extends from $z=0$ to L. t_R denotes the empty-cavity round-trip time $\mathscr{L}/c$, and $\Delta t = (\mathscr{L} - L)/c$. Finally, the cavity is taken to be defined by four mirrors, of which two are perfectly reflecting and two have reflectivity $R<1$. The transmissivity of the latter mirrors is $T = 1-R$. We will later introduce the empty-cavity linewidth, $\kappa = cT/\mathscr{L}$.

We now transform the Maxwell-Bloch equations plus boundary condition into a set of purely real equations by means of a decompostion of variables employed by the authors of Refs. 1 and 2. This transformation has the form

$$E(z,t) = |E(z,t)|\, e^{-i\varphi(z,t)} , \tag{2.6a}$$

$$S_a(z,t) = [u_a(z,t) + iv_a(z,t)]e^{-i\varphi(z,t)} , \tag{2.6b}$$

$$S_b(z,t) = [u_b(z,t) + iv_b(z,t)]e^{-i\varphi(z,t)} , \tag{2.6c}$$

$$\Phi(z,t) = \frac{\partial}{\partial t}\varphi(z,t) . \tag{2.6d}$$

The transformed Maxwell-Bloch equations are then

$$\frac{\partial}{\partial t}|E| = -c\frac{\partial}{\partial z}|E| - g_a u_a - g_b u_b , \tag{2.7a}$$

$$-|E|\Phi = c|E|\frac{\partial\varphi}{\partial z} - g_a v_a - g_b v_b , \tag{2.7b}$$

$$\frac{\partial}{\partial t}u_a = -v_a\Phi - \gamma_{\perp a}u_a + \Delta\omega_a v_a + \frac{\mu_a}{\hbar}D_a|E| , \tag{2.7c}$$

$$\frac{\partial}{\partial t}u_b = -v_b\Phi - \gamma_{\perp b}u_b + \Delta\omega_b v_b + \frac{\mu_b}{\hbar}D_b|E| , \tag{2.7d}$$

$$\frac{\partial}{\partial t}v_a = u_a\Phi - \gamma_{\perp a}v_a - \Delta\omega_a u_a , \tag{2.7e}$$

$$\frac{\partial}{\partial t}v_b = u_b\Phi - \gamma_{\perp b}v_b - \Delta\omega_b u_b , \tag{2.7f}$$

$$\frac{\partial}{\partial t}D_a = -\gamma_{\|a}\frac{N_a}{2} - \gamma_{\|a}D_a - \frac{\mu_a}{\hbar}|E|u_a , \tag{2.7g}$$

$$\frac{\partial}{\partial t}D_b = \gamma_{\|b}\frac{N_b}{2} - \gamma_{\|b}D_b - \frac{\mu_b}{\hbar}|E|u_b . \tag{2.7h}$$

The boundary condition similarly transforms into a pair of equations

$$|E(0,t)| = R\,|E(L,t-\Delta t)| , \tag{2.8a}$$

$$\varphi(0,t) = \varphi(L,t-\Delta t) + \Delta\omega_c t_R . \tag{2.8b}$$

We next express the steady state in terms of the transformed equations by setting all time derivatives to zero. Steady-state forms of the state variables and their transformations are functions only of z and are denoted by the superscript SS. $|E|^{SS}$ is written as $|E^{SS}|$ for legibility. The equations become

$$0 = -c\frac{d}{dz}|E^{SS}| - g_a u_a^{SS} - g_b u_b^{SS} , \tag{2.9a}$$

$$0 = c|E^{SS}|\frac{d}{dz}\varphi^{SS} - g_a v_a^{SS} - g_b v_b^{SS} , \tag{2.9b}$$

$$0 = -\gamma_{\perp a}u_a^{SS} + \Delta\omega_a v_a^{SS} + \frac{\mu_a}{\hbar}D_a^{SS}|E^{SS}| , \tag{2.9c}$$

$$0 = -\gamma_{\perp b}u_b^{SS} + \Delta\omega_b v_b^{SS} + \frac{\mu_b}{\hbar}D_b^{SS}|E^{SS}| , \tag{2.9d}$$

$$0 = -\gamma_{\perp a}v_a^{SS} - \Delta\omega_a u_a^{SS} , \tag{2.9e}$$

$$0 = -\gamma_{\perp b}v_b^{SS} - \Delta\omega_b u_b^{SS} , \tag{2.9f}$$

$$0 = -\gamma_{\|a}\frac{N_a}{2} - \gamma_{\|a}D_a^{SS} - \frac{\mu_a}{\hbar}|E^{SS}|u_a^{SS} , \tag{2.9g}$$

$$0 = \gamma_{\|b}\frac{N_b}{2} - \gamma_{\|b}D_b^{SS} - \frac{\mu_b}{\hbar}|E^{SS}|u_b^{SS} . \tag{2.9h}$$

In the steady state the boundary conditions are

$$|E^{SS}(0)| = R\,|E^{SS}(L)| , \tag{2.10a}$$

$$\varphi^{SS}(0) = \varphi^{SS}(L) + \Delta\omega_c t_R . \tag{2.10b}$$

The last six of the main equations, Eqs. (2.9c)–(2.9h), can be straightforwardly solved for the u's in terms of $|E^{SS}|$, and for the v's and D's in terms of these,

$$u_a^{SS} = -\frac{\mu_a}{2\gamma_{\perp a}\hbar}N_a\frac{|E^{SS}|}{1+(\Delta\omega_a^2/\gamma_{\perp a}^2)+(|E^{SS}|^2/I_{sa})} , \tag{2.11a}$$

$$u_b^{SS}=\frac{\mu_b}{2\gamma_{\perp b}\hbar}N_b\frac{|E^{SS}|}{1+(\Delta\omega_b^2/\gamma_{\perp b}^2)+(|E^{SS}|^2/I_{sb})}\ , \tag{2.11b}$$

$$v_a^{SS}=-\frac{\Delta\omega_a}{\gamma_{\perp a}}u_a^{SS}\ , \tag{2.11c}$$

$$v_b^{SS}=-\frac{\Delta\omega_b}{\gamma_{\perp b}}u_b^{SS}\ , \tag{2.11d}$$

$$D_a^{SS}=-\frac{N_a}{2}-\frac{\mu_a}{\gamma_{\|a}\hbar}|E^{SS}|u_a^{SS}\ , \tag{2.11e}$$

$$D_b^{ss}=+\frac{N_b}{2}-\frac{\mu_b}{\gamma_{\|b}\hbar}|E^{SS}|u_b^{SS}\ . \tag{2.11f}$$

Here we have introduced the "saturation intensities" I_{sa} and I_{sb}, defined as

$$I_{sa}=\frac{\hbar^2\gamma_{\perp a}\gamma_{\|a}}{\mu_a^2} \tag{2.12a}$$

$$I_{sb}=\frac{\hbar^2\gamma_{\perp b}\gamma_{\|b}}{\mu_b^2}\ . \tag{2.12b}$$

The results for the u's can be substituted into Eq. (2.9a), which can then be integrated to yield $|E^{SS}(z)|$ as an implicit function. Equation (2.9b) can be integrated by treating φ^{SS} as a function φ_E^{SS} of $|E^{SS}|$, putting $d\varphi^{SS}/dz=(d\varphi_E^{SS}/d|E^{SS}|)(d|E^{SS}|/dz)$, and substituting for $d|E^{SS}|/dz$ from Eq. (2.9a). Expressing the u's and v's in terms of $|E^{SS}|$ and integrating with respect to $|E^{SS}|$ yields $\varphi_E^{SS}(|E^{SS}|)$. $\varphi^{SS}(z)$ is then defined indirectly through $\varphi_E^{SS}(|E^{SS}|)$ and the implicit function $|E^{SS}(z)|$. The constants of integration may be taken as $|E^{SS}(0)|$ and $\varphi^{SS}(0)$. In this way one obtains the following:

$$p\ln\left[\frac{|E^{SS}(z)|^2}{|E^{SS}(0)|^2}\right]+q\ln\left[\frac{|E^{SS}(z)|^2+k_3/k_4}{|E^{SS}(0)|^2+k_3/k_4}\right]^2+\frac{1}{2k_4}[|E^{SS}(z)|^2-|E^{SS}(0)|^2]=z\ , \tag{2.13a}$$

$$\Delta\varphi_{0z}^{SS}\equiv\varphi^{SS}(z)-\varphi^{SS}(0)=p'z+q'\ln\left[\frac{|E^{SS}(z)|^2+k_3/k_4}{|E^{SS}(0)|^2+k_3/k_4}\right]^2-\frac{p'}{2k_4}[|E^{SS}(z)|^2-|E^{SS}(0)|^2]\ . \tag{2.13b}$$

In the limit $N_b\to 0$, Eq. (2.13a) takes the form of the corresponding equation found by Lugiato *et al.* for the case of the homogeneously broadened ring laser [Eq. (2.12) of Ref. 6]. The coefficients k_n, p, q, p', and q' are defined below; they contain the various parameters of the system and the operating frequency ω_0. These expressions for $|E^{SS}(z)|^2$ and $\Delta\varphi_{0z}^{SS}$ thus require values for $|E^{SS}(0)|^2$ and ω_0. The latter two can be evaluated by setting $z=L$ in Eqs. (2.13) and using the boundary conditions $|E^{SS}(L)|=|E^{SS}(0)|/R$ and $\varphi^{SS}(L)-\varphi^{SS}(0)\equiv\Delta\varphi_{0L}^{SS}=-\Delta\omega_c t_R$. The equations which result are

$$-2p\ln R+q\ln\left[\frac{|E^{SS}(0)|^2/R^2+k_3/k_4}{|E^{SS}(0)|^2+k_3/k_4}\right]^2+\frac{1}{2k_4}(1/R^2-1)|E^{SS}(0)|^2=L\ , \tag{2.14a}$$

$$\Delta\varphi_{0L}^{SS}\equiv\varphi^{SS}(L)-\varphi^{SS}(0)=-\Delta\omega_c t_R=p'L+q'\ln\left[\frac{|E^{SS}(0)|^2/R^2+k_3/k_4}{|E^{SS}(0)|^2+k_3/k_4}\right]^2-\frac{p'}{2k_4}(1/R^2-1)|E^{SS}(0)|^2\ . \tag{2.14b}$$

Corresponding values of $|E^{SS}(0)|^2$ and ω_0 appear as the simultaneous roots of these two transcendental equations; we cannot obtain a convenient "mode-pulling equation" for ω_0 without further approximation. In general, we expect multiple pairs of roots from these equations. We now define the coefficients used in these expressions. First let c_1, c_2, d_1, and d_2 be as follows:

$$c_1=\frac{\hbar N_a g_a\gamma_{\|a}}{2\mu_a c}\equiv\frac{2\pi\hbar N_a\gamma_{\|a}\omega_0}{cV}\ , \tag{2.15a}$$

$$c_2=(\hbar^2/\mu_a^2)\frac{\gamma_{\|a}}{\gamma_{\perp a}}(\gamma_{\perp a}^2+\Delta\omega_a^2)\ , \tag{2.15b}$$

$$d_1=-\frac{\hbar N_b g_b\gamma_{\|b}}{2\mu_b c}\equiv-\frac{2\pi\hbar N_b\gamma_{\|b}\omega_0}{cV}\ , \tag{2.15c}$$

$$d_2=(\hbar^2/\mu_b^2)\frac{\gamma_{\|b}}{\gamma_{\perp b}}(\gamma_{\perp b}^2+\Delta\omega_b^2)\ . \tag{2.15d}$$

Then we define

$$\begin{aligned}&k_1=c_2d_2,\quad k_2=c_2+d_2\ ,\\&k_3=c_1d_2+d_1c_2,\quad k_4=c_1+d_1\ ,\\&k_5=\frac{\Delta\omega_a}{\gamma_{\perp a}}c_1d_2+\frac{\Delta\omega_b}{\gamma_{\perp b}}c_2d_1\ ,\\&k_6=\frac{\Delta\omega_a}{\gamma_{\perp a}}c_1+\frac{\Delta\omega_b}{\gamma_{\perp b}}d_1\ ,\end{aligned} \tag{2.16}$$

and

$$\begin{aligned}&p=\frac{k_1}{2k_3},\quad p'=\frac{k_5}{k_1}\ ,\\&q=\frac{1}{4}\frac{k_2k_3k_4-k_1k_4^2-k_3^2}{k_3k_4^2}\equiv\frac{c_1d_1(c_2-d_2)^2}{4k_3k_4^2}\ ,\\&q'=\frac{1}{4}\frac{k_3k_5-k_2k_4k_5+k_1k_4k_6}{k_1k_4^2}\ .\end{aligned} \tag{2.17}$$

III. STEADY-STATE SOLUTIONS IN THE UNIFORM-FIELD APPROXIMATION

The preceding results may be simplified greatly by applying the uniform-field approximation.[7(a)] As is usual in uniform-field treatments, the excitation of each medium is expressed by a "lumped parameter" containing the ratio of the number N of active atoms to the mirror transmis-

sivity T, multiplied by the cell length L. For the amplifying and absorbing media, we define these, respectively, by

$$A=\frac{2\pi\hbar}{c}\frac{\gamma_{\parallel a}}{V}\frac{N_a L}{T}\omega_0\equiv(L/T)c_1\ , \tag{3.1a}$$

$$B=\frac{2\pi\hbar}{c}\frac{\gamma_{\parallel b}}{V}\frac{N_b L}{T}\omega_0\equiv-(L/T)d_1\ . \tag{3.1b}$$

We will later refer to A and B as the "excitation parameters" for the system, or simply as the "excitations" of the respective media. Eventually we will specify a value for B, and will then sometimes refer to A alone as the excitation parameter or merely as the excitation. The uniform-field approximation amounts to a limiting procedure in which $N_a L\to 0$, $N_b L\to 0$, and $T\to 0$, while A and B are fixed at chosen finite values. It is also assumed that the lumped parameters A and B can be maintained constant or varied independently of other parameters, even though some quantities, such as ω_0, may vary with operating conditions. Physically, this limiting process corresponds to making the media optically thin while decreasing the nonsaturable losses in the cavity, in such a way that the intensity remains finite. In this limit, the state variables become independent of position z, and, when appropriately defined, of the individual values of T, L, N_a, and N_b.

The uniform-field approximation is typically applied to the fundamental semiclassical or quantum equations used in the model before attempting to solve them, thereby eliminating the troublesome z derivative of the electric field. This method is used in Refs. 1(a) and 2(b). In our approach, we apply it instead to the longitudinally dependent solutions found above. We do this by first expanding our solutions (2.14) for $|E^{\rm SS}(0)|^2$ and $\Delta\varphi_{0L}^{\rm SS}$ in powers of T. We anticipate that terms in powers of T higher than the first will be eradicated by the limiting process, and drop these immediately. With one exception, the remaining first powers of T can be combined with the quantities L, $N_a\omega_0$, and $N_b\omega_0$, and thus be absorbed into the constant parameters A and B. The exception occurs in the uniform-field expression for the total phase shift $\Delta\varphi_{0L}^{\rm SS}$, which retains an overall proportionality to T. However, we shall find that we can work instead with the quantity $G(\omega_0)\equiv(\Delta\varphi_{0L}^{\rm SS}/T)$, which we call the "phase-shift—transmissivity ratio," or, when the context is clear, the "phase-shift function." This total quantity remains finite in the uniform-field limit, and is independent of the separate values of T, L, N_a, and N_b, but does depend on the lumped parameters A and B. The physical significance of this behavior of $\Delta\varphi_{0L}^{\rm SS}$ is that it becomes proportional to the number of active atoms in the medium as the medium becomes optically thin.

The end results of this process are the following equations. For notational clarity, the superscript SS is changed to UF to indicate that the uniform-field limit has been taken. There is no longer any z dependence. The implicit function for $|E^{\rm SS}(0)|^2$, Eq. (2.14a), becomes a quadratic equation defining $|E^{\rm UF}|^2$,

$$|E^{\rm UF}|^4+[(c_2+d_2)-(A-B)]\,|E^{\rm UF}|^2 +[c_2d_2-(Ad_2-Bc_2)]=0\ . \tag{3.2}$$

This has solutions,

$$|E^{\rm UF}|^2_{\pm}=\tfrac{1}{2}[-P\pm(P^2-4Q)^{1/2}] \tag{3.3a}$$

with

$$P=[(c_2+d_2)-(A-B)]\ , \tag{3.3b}$$

$$Q=[c_2d_2-(Ad_2-Bc_2)]\ . \tag{3.3c}$$

From these equations it follows that

$$|E^{\rm UF}|^2_{+}\geqq|E^{\rm UF}|^2_{-} \tag{3.4}$$

for all values of ω_0 where two real roots exist. Setting $|E^{\rm UF}|^2=0$ in Eq. (3.2) gives the value of the amplifying-medium excitation parameter A at the lasing threshold. In the limit of zero absorption ($B\to 0$, $N_b\to 0$), we find that the minimal threshold is $A=I_{sa}$, which occurs for $\omega_0=\omega_a$ (a tuned, homogeneously broadened ring laser). Note that the boundary condition on E is no longer relevant in the uniform-field treatment.

In this way we have obtained a "state relation" for the squared electric field amplitude as a function of the laser operating frequency. Applying this method to equation (2.14b) for the total phase shift due to the medium gives the function for the phase-shift—transmissivity ratio in the uniform-field approximation,

$$\begin{aligned}G_{\pm}(\omega_0)&\equiv\Delta\varphi_{0L\pm}^{\rm UF}/T\\&=\frac{1}{\gamma_{\perp a}\gamma_{\perp b}(c_2-d_2)}\\&\quad\times[(A-B-|E^{\rm UF}|^2_{\pm})(\gamma_{\perp b}\Delta\omega_a-\gamma_{\perp a}\Delta\omega_b)\\&\quad+(\gamma_{\perp a}c_2\Delta\omega_b-\gamma_{\perp b}d_2\Delta\omega_a)]\ .\end{aligned} \tag{3.5a}$$

As in the derivation of Eq. (2.14b), the boundary condition on the total phase shift requires

$$G_{\pm}(\omega_0)=-\Delta\omega_c t_R/T=-\Delta\omega_c/\kappa\ . \tag{3.5b}$$

Here we treat the empty-cavity linewidth $\kappa=cT/\mathscr{L}\equiv T/t_R$ as a third parameter of the system to be held fixed when the uniform-field limit is taken. This makes sense physically as an approximation to the properties of a real cavity with highly reflective mirrors (see the discussion of parameter values in Sec. IV). Then Eq. (3.5b) is the mode-pulling equation for this system in the uniform-field approximation, and allows us to find the possible steady-state operating frequencies as functions of the cavity tuning, contained within $\Delta\omega_c$. From these, and the equation for $|E^{\rm UF}|^2_{\pm}$, we can find the corresponding electric fields. In addition, for a given tuning, we can find the dependence of operating frequency and electric field on laser excitation, as expressed by the parameters A and B. The question of calculating uniform-field values for the other state variables is taken up in a subsequent paper in connection with the stability problem for the steady-state solutions.[25] We will refer to $|E^{\rm UF}|^2_{+}$ and G_{+} as "primary" solutions, and to $|E^{\rm UF}|^2_{-}$ and G_{-} as "secondary" solutions.

In carrying out this program, much insight is gained by first considering Eqs. (3.3) and (3.5a) for $|E^{\rm UF}|^2_{\pm}(\omega_0)$ and

$G_{\pm}(\omega_0)$ as "state relations" which are independent of the boundary condition (3.5b). The boundary condition can then be treated as a constraint on the permitted values of the phase-shift function $G_{\pm}(\omega_0)$. We have

$$G_{\pm}(\omega_0) = -\Delta\omega_c/\kappa = (\omega_0 - \omega_c)/\kappa \ . \tag{3.5c}$$

Thus this constraint corresponds to a straight line on a plot of the phase-shift—transmissivity ratio versus operating frequency, whose intersections with the phase-shift function give the physically allowed solutions for $G_{\pm}$ and ω_0. The line's intercept with the frequency axis is the cavity tuning, that is, the frequency ω_c of the empty-cavity mode closest in frequency to the operating frequency. When frequency is presented as angular frequency, as here, the slope of such a "mode line" is the reciprocal of the empty-cavity linewidth κ. Finally, the allowed values of ω_0 determine corresponding allowed values of $|E^{\mathrm{UF}}|^2$ through the expression for $|E^{\mathrm{UF}}|^2_{\pm}(\omega_0)$.

Neither the cavity tuning nor the cavity linewidth, as such, enters the expressions for $|E^{\mathrm{UF}}|^2_{\pm}(\omega_0)$ and $G_{\pm}(\omega_0)$ given by Eqs. (3.3) and (3.5a). The dependence of the solutions on cavity tuning can therefore be obtained by translating or "sweeping" a mode line horizontally across a plot of the phase-shift—transmissivity ratio versus operating frequency. Similarly, their dependence on cavity linewidth can be obtained merely by varying the slope of the mode line. On the other hand, variation of the excitation of the media, expressed by the parameters A and B, distorts the plots of $|E^{\mathrm{UF}}|^2_{\pm}(\omega_0)$ and $G_{\pm}(\omega_0)$, but leaves the mode line unaffected.[26] Results obtained from the numerical realization of these procedures will be discussed in Secs. IV—VI. It is in the development of these solutions from the uniform-field approximation that the spirit of our approach owes most to the paper by Casperson and Yariv referred to above.[23] A more formal alternative is to use Eqs. (3.3) and (3.5a) to rearrange the mode-pulling equation (3.5c). This gives a polynomial equation of the sixth degree in the operating frequency. Then three of the mathematically possible roots correspond to possible intersections of the mode line with the primary phase-shift—transmissivity curve, and three to possible intersections with the secondary curve.

IV. CALCULATION OF STEADY-STATE SOLUTIONS FOR THE CASE OF MEDIA HAVING THE SAME LINE-CENTER FREQUENCY

The solutions found above are so complicated in form that it is necessary to plot the results of calculations using typical parameter values in order to visualize the relationships. In this and Secs. V and VI we present an analysis of such results, generated by using the state-relation—mode-line method developed in Sec. III. Thus we assign physically reasonable parameter values, calculate the state relations, and numerically find intersections of the chosen mode line with the curve of the phase-shift—transmissivity ratio. These intersections define operating frequencies and, via the state relations, the corresponding values of squared electric field. By varying relevant parameters, we are then able to generate plots of squared electric field and operating frequency versus cavity tuning and excitation of the amplifying medium. We also examine how these plots are affected by changes in the cavity linewidth. Initially we treat the case in which the amplifying and absorbing atoms have a common resonance frequency. The results are presented graphically in Figs. 2—5 and are discussed in detail below and in Sec. V.

In the following, electrical quantities are expressed in the electrostatic (ESU) system of units. The parameter values used are line-center wavelength, 3.51 μm; decay rates for amplifying-medium polarization and population inversion, $\gamma_{\perp a}$ and $\gamma_{\parallel a}$, 100×10^6 sec^{-1}; for the absorbing medium $\gamma_{\perp b}$ and $\gamma_{\parallel b}$, 10×10^6 sec^{-1}; electric dipole transition moments μ_a and μ_b, 2.17×10^{-17} and 0.434×10^{-17} cm$^{5/2}$ g$^{1/2}$ sec^{-1}. The values for the line-center wavelengths and for the transition moment of the amplifying medium are those for a known lasing transition in xenon.[27] The other values have been chosen simply for convenience, as well as physical reasonableness. Those for the absorbing medium give it a linewidth one-tenth that of the amplifying medium, and a transition moment one-fifth as great. These parameter values give saturation intensities $I_{sa}=2.36\times10^{-5}$ g cm^{-1} sec^{-2} and $I_{sb}=5.90\times10^{-6}$ g cm^{-1} sec$^{-2}=(I_{sa}/4)$.

Levels of excitation of the amplifying and absorbing

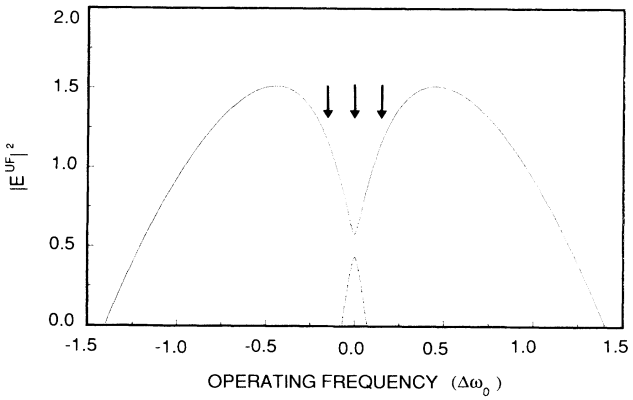

FIG. 2. Squared electric field vs relative operating frequency $\Delta\omega_0$ for $\Delta\omega_{ab}=0$ (that is, amplifying and absorbing media have the same line-center frequency). In this plot the amplifying medium excitation parameter is $A=3.02I_{sa}$. In all figures, operating frequency, cavity detuning, cavity linewidth, and line center offset $\Delta\omega_{ab}$ are expressed in units of the amplifying medium polarization decay rate $\gamma_{\perp a}=100\times10^6$ sec^{-1}. Similarly, squared electric field and the amplifying medium excitation parameter A are always presented in units of $I_{sa}=2.36\times10^{-5}$ g cm^{-1} sec^{-2}. The primary solutions in every figure are drawn as solid curves, and the secondary solutions as dashed curves. These curves and those of Fig. 3 exemplify the state relations discussed in Secs. III and IV of the text. If the value of the excitation parameter is not too high, the plot of the primary solution for squared electric field shows a pair of maxima and, if continuous, a minimum at $\Delta\omega_0=0$. The plot of the corresponding secondary solution has a maximum at the same location if it is greater than zero there. The arrows indicate the possible operating frequencies and the corresponding values of squared electric field obtained by the method of Casperson and Yariv for the mode line illustrated in Fig. 3.

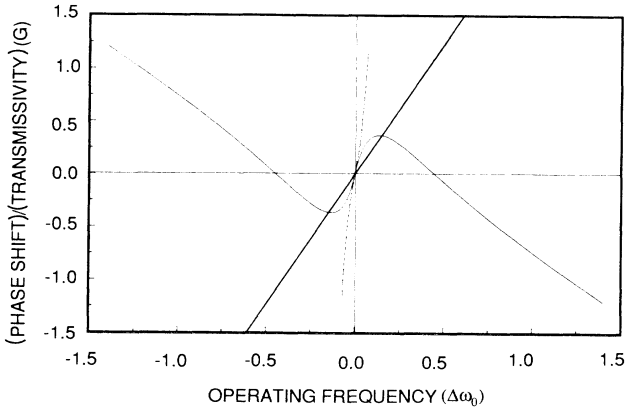

FIG. 3. The phase-shift—transmissivity ratio vs operating frequency $\Delta\omega_0$ for $\Delta\omega_{ab}=0$ and the same A value as in Fig. 2 ($A=3.02I_{sa}$). The primary solution is represented by a solid curve, and the secondary solution by a dashed curve. The primary solution shows a minimum and a maximum on its region of physical existence when it is continuous, while the secondary solution is monotonic on the region where it has physical existence. The solid straight line is an example of a mode line used in the method of Casperson and Yariv. It corresponds to a detuning of zero and a cavity linewidth of $\kappa=0.40\gamma_{\perp a}$; thus its horizontal intercept is zero and its slope is $\kappa^{-1}=2.5$ in the units employed for the plot. Its intersections with the curves gave the possible steady-state operating frequencies for the parameter values chosen. These operating frequency values were used in conjunction with the curves of Fig. 2 to obtain the corresponding values of squared electric field; they are indicated by the arrows in Fig. 2. Shifting the intercept of the mode line gave the results for variable detuning shown in Figs. 4(a) and 4(b) for this value of cavity linewidth. Leaving the mode line fixed and varying the amplifier excitation gave the results for zero detuning presented in Figs. 5(a) and 5(b). The slope of the mode line was changed to obtain the results for other linewidth values shown in Figs. 4(c)—4(f), and various combinations of linewidth and detuning with variable excitation gave the remaining results shown in Fig. 5. For further explanation of the mode line method, see Sec. III of the text.

media are respectively represented by the parameters A and B defined in Eqs. (3.1). We take $B=1.779\times10^{-5}$ g cm^{-1} sec$^{-2}=(0.754)I_{sa}=(3.02)I_{sb}$ throughout the calculations presented here. This value of B corresponds to $T=0.01$, $L=15.0$ cm, $V=1.0$ cm^3, $N_b=1.0\times10^7$, and $\omega_0=\omega_a=5.37\times10^{14}$ sec^{-1}. Since $\gamma_{\|a}=10\gamma_{\|b}$, $A=10(N_a/N_b)B$ for the values we are using. Having fixed B, for the sake of brevity we will sometimes use the unqualified terms excitation and excitation parameter to refer to the value of A alone. Because of the uniform-field treatment, our results do not depend on the individual values of T, L, N_a, and N_b, but rather on the lumped parameters A and B.

For $T=0.01$ and $\mathscr{L}=30.0$ cm, the cavity linewidth $\kappa=10.0\times10^6$ sec^{-1}. In the uniform-field treatment, κ is also considered as an independent lumped parameter; thus we will later introduce cavity linewidth values ranging from 6.5×10^6 to 40.0×10^6 sec^{-1}. These are of the same order as the decay rates for the absorbing medium, but the lower values are an order of magnitude smaller than the decay rates for the amplifying medium.

In order to express our results in a more convenient and general form, we adopt the following conventions for the graphical presentation of numerical results. All optical frequencies are given as angular frequencies relative to the amplifying atom line center ω_a, using the relative frequencies defined in Eqs. (2.4). Thus operating frequency is expressed as $\Delta\omega_0$, the absorbing medium line center as $\Delta\omega_{ab}$, and the cavity tuning as the detuning $\Delta\omega_{ac}$. These and the cavity linewidth κ will be expressed in units of $\gamma_{\perp a}$. Similarly, we shall express values of $|E^{\rm UF}|^2_{\pm}$ in units of the amplifier saturation intensity I_{sa}. We note that for a plane wave, $|E|^2=1.0\times10^{-5}$ g cm^{-1} sec^{-2} corresponds to an intensity of $(c/8\pi)|E|^2=1.19$ mW cm^{-2}, so that here $|E|^2=I_{sa}$ corresponds to an intensity of 2.81 mW cm^{-2}. As mentioned in the comments following Eqs. (3.2)—(3.4), for a cavity tuned to the amplifying medium line center, $A=I_{sa}$ is the lasing threshold in the absence of an absorbing medium. Therefore we shall also express the amplifier excitation A in units of I_{sa}. The values of $\gamma_{\perp a}$, I_{sa}, I_{sb}, and B are the same throughout the calculations presented in this paper.

Examples of the state relations discussed in Sec. III are plotted in Figs. 2 and 3. Figure 2 shows a plot of squared electric field versus operating frequency for a specific value of the amplifying medium excitation parameter A. For this value of A, both the primary and the secondary solutions are physically meaningful and are continuous over their range of physical existence. For all values of A, the primary solution (solid curve) has the larger intensity at a given frequency, and spans a wider range of operating frequency, while the lower-intensity secondary solution (dashed curve) has physical existence over a much narrower range of operating frequencies near the absorber line center. The secondary solution also exists over a narrower range of values of the excitation parameter A; if A is raised or lowered sufficiently, the secondary solution disappears while the primary one may still exist [cf. Figs. 5(a) and 5(b)]. For the case in which the media are in resonance, such plots of squared electric field are symmetric about the common line-center frequency of the two media.

For values of A which are sufficiently below that used in Fig. 2, there is an intermediate region of operating frequency for which the laser is below threshold. In such a case, both the primary and secondary solutions are discontinuous functions of operating frequency. If A is low enough, the secondary solution is completely unphysical. For still lower values of A, the primary solution also becomes unphysical; the laser is below threshold for all operating frequencies. For intermediate values of A, as exemplified in Fig. 2, both solutions have continuous domains of existence. The maximum value of the secondary solution now decreases with increasing A while the local minimum of the primary solution increases in value. Finally, at sufficiently high values of A, the secondary solution fades away completely, and is again unphysical for all values of operating frequency. These general features are also seen in the plots of $|E^{\rm UF}|^2$ versus A presented in Fig. 5.

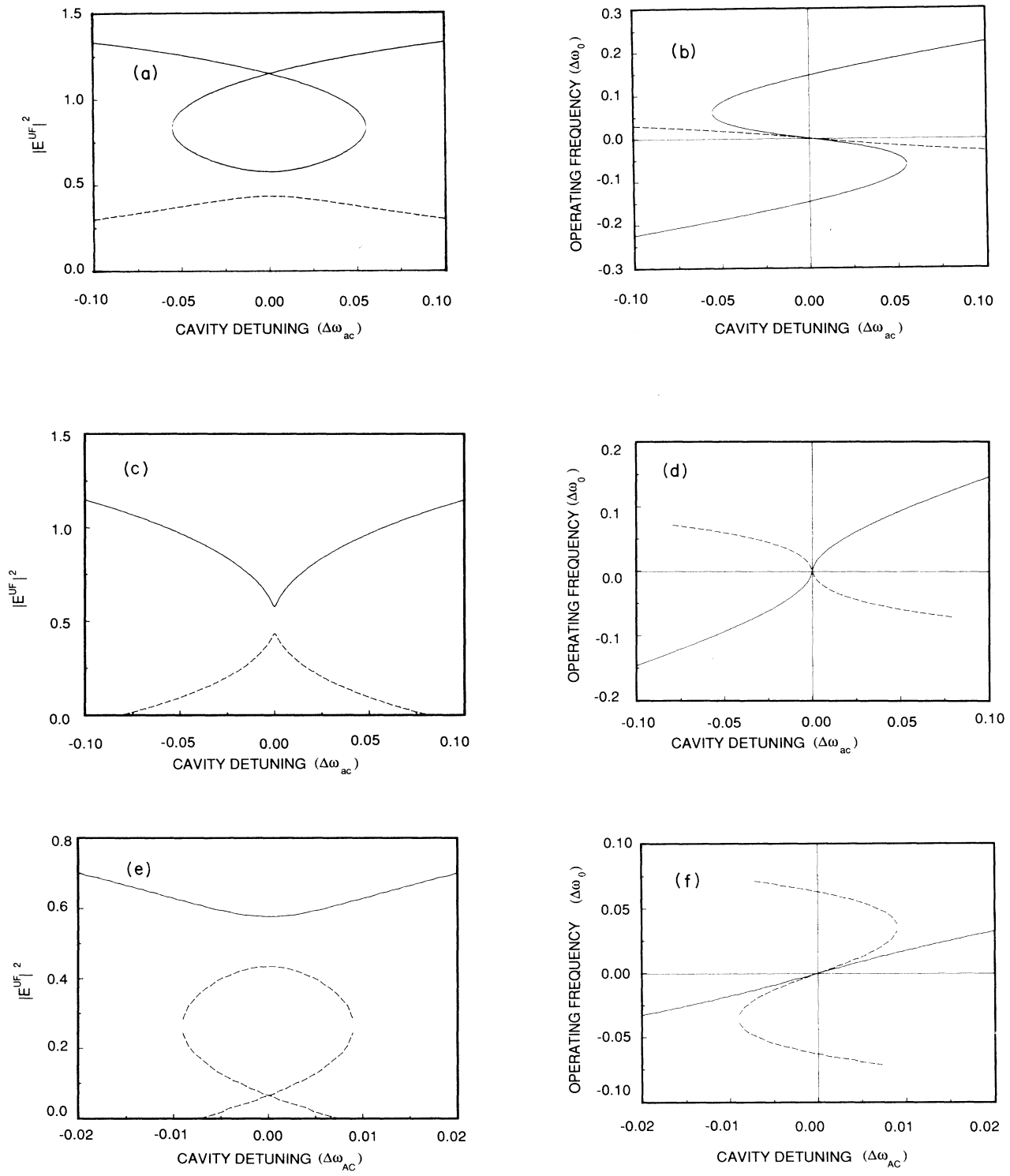

FIG. 4. Squared electric field (a), (c), and (e) and operating frequency $\Delta\omega_0$ (b), (d), and (f) vs the detuning $\Delta\omega_{ac}$, for $\Delta\omega_{ab}=0$. Here $A=3.02I_{sa}$, corresponding to Figs. 2 and 3. Cavity linewidths are (a) and (b), $\kappa=0.40\gamma_{\perp a}$; (c) and (d), $\kappa=0.125\gamma_{\perp a}$; and (e) and (f), $\kappa=0.065\gamma_{\perp a}$. These plots were obtained from the data of Figs. 2 and 3 by means of the mode-line-intersection procedure described in Sec. III of the text and exemplified in Figs. 2 and 3. Branches given by the primary and secondary solutions are shown as solid and dashed curves, respectively. Breaks in the curves are numerical artifacts occurring between the contiguous branches of multivalued solutions.

The primary and secondary solutions for the field each have a corresponding solution for the phase-shift—transmissivity ratio as a function of operating frequency. These are plotted in Fig. 3. It must be emphasized that this phase shift applies to the steady-state laser radiation itself, at the intensity level found on Fig. 2 at each particular operating frequency, for the primary and secondary solutions. These curves would not be observed for a weak beam injected externally and passing once through the medium cell. In other words, saturation of the active media by the intense circulating field is properly taken into account. Figure 3 shows primary and secondary solutions for the phase-shift—transmissivity ratio corresponding to the solutions of Fig. 2. When the media have a common resonance frequency, these curves have centers of inversion at that frequency.

The usefulness of the mode-line analysis described in Sec. III is nicely shown by the typical case illustrated in Figs. 2 and 3. The value of the excitation A for these curves is such that primary and secondary solutions each exist over a continuous domain of operating frequency containing the absorption maximum. Then the branches of the phase-shift function both exist in this region without breaks. In such a case, we find that as the slope of the mode line increases from values near zero, the maximum numbers of intersections with the branches of the phase-shift—transmissivity ratio change according to the following pattern: for low values of slope, there are up to three intersections with the primary branch and one with the secondary; for a narrow intermediate range, at most

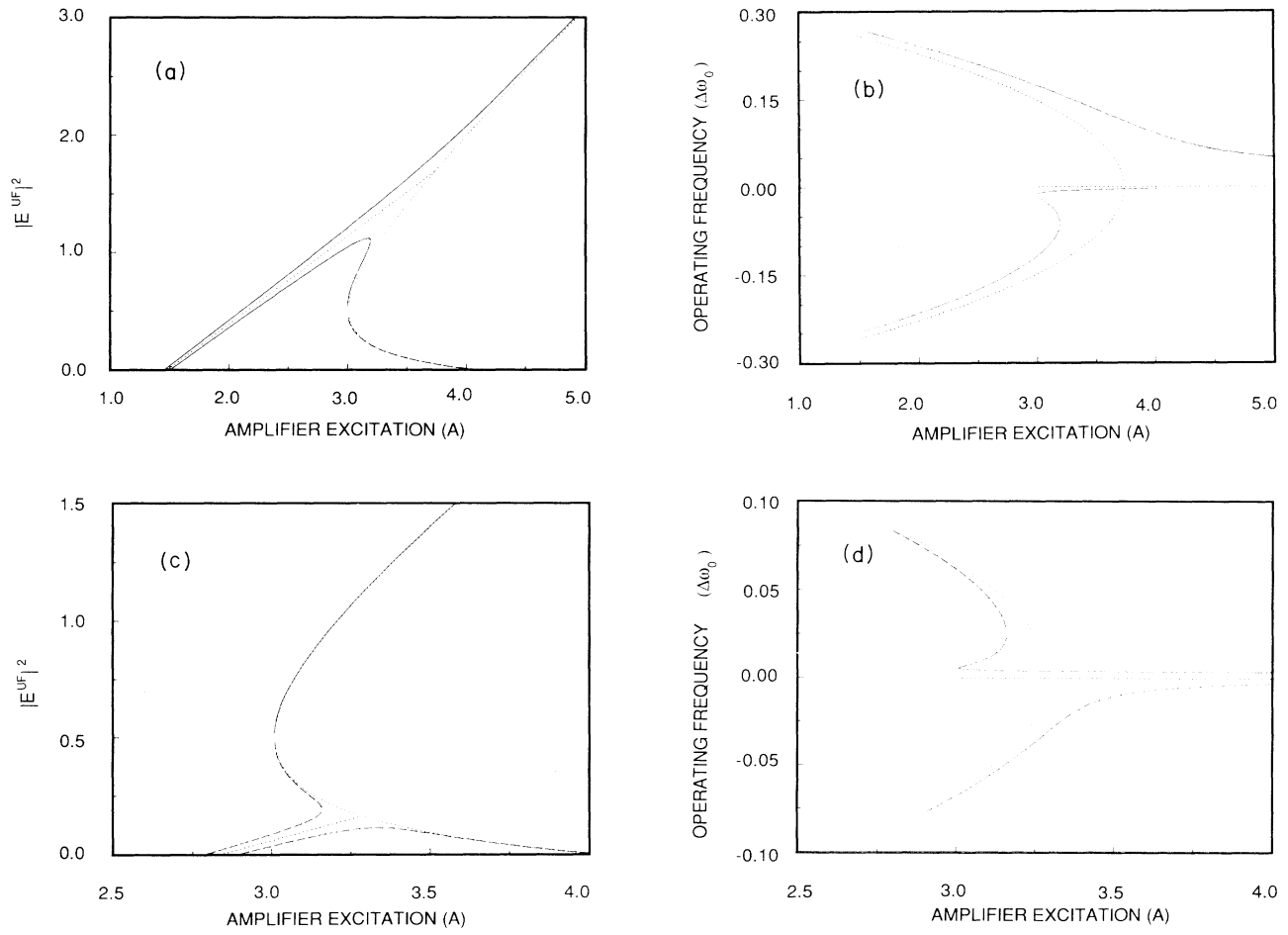

FIG. 5. Squared electric field (a) and (c) and operating frequency $\Delta\omega_0$ (b) and (d) vs amplifying medium excitation parameter for $\Delta\omega_{ab}=0$. The cavity linewidths and detunings are (a) and (b), $\kappa=0.40\gamma_{\perp a}$; $\Delta\omega_{ac}=0.0\gamma_{\perp a}$ is shown by dotted curves, and $\Delta\omega_{ac}=0.030\gamma_{\perp a}$ is shown by solid curves for primary solutions and dashed curves for secondary solutions; and (c) and (d), $\kappa=0.065\gamma_{\perp a}$; $\Delta\omega_{ac}=0.0\gamma_{\perp a}$ is shown by dotted curves, and $\Delta\omega_{ac}=2.5\times10^{-3}\gamma_{\perp a}$ is shown by solid curves for primary solutions and dashed curves for secondary solutions. Sections through the plots of (a) and (b) at $A=3.02I_{sa}$ correspond to sections through the plots of Figs. 4(a) and 4(b) at cavity-detuning values of $\Delta\omega_{ac}=0.0\gamma_{\perp a}$ and $\Delta\omega_{ac}=0.030\gamma_{\perp a}$. Sections through the plots of (c) and (d) at $A=3.02I_{sa}$ correspond to sections through the plots of Figs. 4(e) and 4(f) at cavity detuning values of $\Delta\omega_{ac}=0.0\gamma_{\perp a}$ and $\Delta\omega_{ac}=2.5\times10^{-3}\gamma_{\perp a}$. The curves in the case of the tuned cavity show degeneracies with respect to squared electric field and operating frequency which are broken by detuning. See the text for a discussion of this.

one intersection with each branch; and for higher values of slope, at most one with the primary branch and as many as three with the secondary. A different pattern results if there is only a discontinuous primary branch (very low A), or if both the primary and secondary branches are physical but discontinuous (low A), or if there is only a continuous primary branch (high A).

Each operating frequency found in this way defines a value for the electric field via the plot in Fig. 2. Intersections on the primary or secondary branch in Fig. 3 give solutions on the corresponding branch in Fig. 2. It is now possible to plot these solutions for squared electric field and operating frequency against cavity tuning by numerically solving the problem for a range of tuning values. Such solutions are shown in Figs. 4(a)—4(f) for three values of the cavity linewidth and the same value of excitation used in Figs. 2 and 3. These results illustrate the pattern noted above, and are discussed in Sec. V. One can also fix the cavity tuning and carry out the computation for a range of amplifier excitation. Solutions for squared electric field and operating frequency versus the excitation parameter A are presented in Figs. 5(a)—5(d) for various combinations of cavity tuning and linewidth. These are also discussed below.

V. VARIABLE TUNING AND EXCITATION FOR MEDIA WITH THE SAME LINE-CENTER FREQUENCY

Figures 4(a)—4(f) show steady-state solutions for the squared electric field and the corresponding operating frequency as functions of cavity tuning and excitation of the amplifying medium, for the case in which the amplifying and absorbing media have a common line-center frequency. In these plots, the cavity tuning is expressed as detuning from the amplifying medium line center, as defined in Eq. (2.4c), and is given in units of $\gamma_{\perp a}$. The effect of cavity linewidth on these plots is striking. In particular, they show the pattern of multiple steady-state solutions described above, as the slope of the mode line increases with decreasing cavity linewidth. The linewidth values are $0.40\gamma_{\perp a}$, $0.125\gamma_{\perp a}$, and $0.065\gamma_{\perp a}$ (that is, 40.0×10^6, 12.5×10^6, and 6.5×10^6 sec^{-1}), in Figs. 4(a) and (4b), 4(c) and 4(d), and 4(e) and 4(f), respectively. These solutions appear in a sudden, bifurcationlike fashion, as the cavity detuning is scanned. These features suggest the possible appearance of bistability, hysteresis, instabilities, jumps in intensity and frequency, multiple frequencies, and pulsing in the tuning behavior of the laser. Such speculations are complicated by the nonlinearity of the system, which prevents a linear combination of solutions from being itself a solution. We are conducting a stability analysis of these solutions in order to clarify such questions, and will report the results elsewhere. The plots for squared electric field are symmetric about zero detuning (cavity tuned to amplifying atom line center), and the plots of operating frequency have inversion centers at zero detuning. In all these plots, the amplifier excitation $A=3.02I_{sa}$, corresponding to Figs. 2 and 3. Small breaks in the curves are numerical artifacts occurring at the ends of single-valued branches.

Figures 5(a)—5(d) show plots of the steady-state squared electric field and operating frequency versus excitation. Figures 5(a) and 5(b) illustrate the case when the cavity linewidth is $0.40\gamma_{\perp a}$, for cavity detunings of 0.0 $\gamma_{\perp a}$ (dotted line) and 0.030 $\gamma_{\perp a}$ (3.0×10^6 sec^{-1}) (solid and dashed lines, indicating primary and secondary branches, respectively). Sections through these curves at an excitation parameter value of $3.02I_{sa}$ correspond to sections through the plots of Figs. 4(a) and 4(b) at detuning values of $0.0\gamma_{\perp a}$ and $0.030\gamma_{\perp a}$. Again one has multiple solutions, with solutions appearing, disappearing, or merging as one scans the value of the excitation parameter. Similar observations apply to Figs. 5(c) and 5(d), which show the case for a cavity linewidth of $0.065\gamma_{\perp a}$, and cavity detuning of 0.0 $\gamma_{\perp a}$ (dotted curves) and 2.5×10^{-3} $\gamma_{\perp a}$ (0.25×10^6 sec^{-1}) (solid and dashed curves). Sections of these plots at an excitation value of $3.02I_{sa}$ are likewise comparable to sections of Figs. 4(e) and 4(f) for corresponding detuning values. As above, the cavity linewidth has a notable effect on the shape of these plots. However, the effect of detuning in this case is particularly remarkable.

In the case of variable excitation with zero detuning, there is a pair of solutions which are degenerate with respect to squared electric field but not with respect to operating frequency. These are the first solutions to appear as the excitation parameter A is increased from zero, and they appear simultaneously. At a higher value of A, a second pair appears. These are degenerate in operating frequency but not in squared electric field. (In fact, this operating frequency is the line-center frequency of the atoms, equal to the cavity tuning.) For cavity linewidths above or below an intermediate value, both pairs of steady-state solutions have mathematical existence over a range of excitation parameter values. As the excitation increases, the initial pair converges in frequency to the frequency of the atomic line centers and the cavity tuning, and disappears at a point on the plot where all branches of solutions meet. Finally, the low-field member of the second pair fades out and only the high-field solution persists at sufficiently high values of excitation. Solutions of just this type have already been described by other authors in the case of zero detuning.[2(a)—2(d),3(a)]

The effect of detuning the cavity away from the line-center frequency of the media is to split both types of degeneracy. Thus, as the excitation parameter A increases from zero, two branches of solutions having different intensities appear at slightly different values of the excitation parameter. These branches never meet at a common point, but instead separate further as the excitation increases. As the excitation becomes high enough, the high-intensity branch persists while the low-intensity branch disappears, as in the tuned case. For sufficiently high cavity linewidth, the low-intensity branch is multivalued, both in intensity and in operating frequency, while for sufficiently low cavity linewidth this is true of the high-intensity branch instead. For low cavity linewidth, the plot of operating frequency versus excitation parameter shows that a jump in intensity in the detuned system is always accompanied by a jump in frequency; this is not necessarily the case in the correspond-

ing tuned system. (See Fig. 5.)

Because of the lifting of degeneracy and the splitting of the plot into nonintersecting branches, one may expect detuning to affect strongly the stability properties of the steady-state solutions. For example, over a range of excitation giving sufficiently low intensity, the tuned case has been shown to admit stable low-amplitude periodic solutions at a frequency which is essentially the beat frequency of two degenerate steady-state solutions.[1(c),2(c),2(d),2(f),3(b),4] Although the coexistence of two steady-state solutions is not possible in a nonlinear system, this result indicates the existence of a solution which approximates such a situation. We suggest that such solutions might not exist, or might not be stable, in the nondegenerate case. Since the degeneracy is broken by any small but finite detuning, one expects some such effects always to be present, due to the practical difficulty of achieving perfect tuning. Thus a study of the properties of the detuned system may be necessary to an understanding of the actual behavior of an experimental "tuned" system. Conversely, one might seek to use these effects to monitor detuning, or to limit it in a hybrid system containing an external feedback loop.

VI. STEADY-STATE SOLUTIONS FOR MEDIA HAVING DIFFERENT LINE-CENTER FREQUENCIES

Selected results for steady-state solutions in which the amplifying and absorbing media have different line-center frequencies are shown in Figs. 6—8. These have been plotted for an absorption line center 100×10^6 sec^{-1} higher in angular frequency than the amplification line center at 3.51 μm (that is, $\Delta\omega_{ab}=\gamma_{\perp a}$). Frequencies are again given as angular frequencies relative to the amplifying medium line center, in units of $\gamma_{\perp a}$. The values of B, I_{sa}, and the other fixed parameters are also the same as before.

Figures 6(a) and 6(b) show state-relation plots of squared electric field and the phase-shift—transmissivity ratio versus operating frequency for a particular value of the excitation parameter A. These are essentially asymmetric versions of the plots of Figs. 2 and 3. The comments made in Sec. IV on the behavior of the primary and secondary solutions as A is varied apply to the nonresonant case as well.

Plots of the squared electric field and operating frequency versus cavity detuning are given in Figs. 7(a)—7(f) for the same cavity linewidths used for Figs. 4(a)—4(f), respectively. The value of the amplifier excitation parameter for these plots is $4.90I_{sa}$. These curves are topologically like those found when the media had the same line-center frequency, but are now asymmetric. Because of this asymmetry, the low-intensity (secondary) branch for the cavity linewidth value of $0.125\gamma_{\perp a}$ becomes multivalued [Figs. 7(c) and 7(d); compare Figs. 4(c) and 4(d)]. On the other hand, the corresponding branch for a cavity linewidth of $0.065\gamma_{\perp a}$ is reduced from being triple valued in Figs. 4(e) and 4(f) to being double valued in Figs. 7(e) and 7(f).

The most interesting new result is the excitation parameter scan shown in Fig. 8. Here both squared electric field and operating frequency are plotted against the excitation A for a cavity detuning of $1.57\gamma_{\perp a}$ (1.57×10^6 sec^{-1}) and a cavity linewidth of $0.40\gamma_{\perp a}$. Figure 8 is to be compared with Figs. 5(a) and 5(b), discussed in Sec. V. The plot of operating frequency versus excitation in Fig. 8(b) is qualitatively similar to that in Fig. 5(b) for a cavity detuning of $2.5\times10^{-3}\gamma_{\perp a}$. These show the presence of two separate branches of solutions, one of which is multivalued. Thus the crossover point on the plot of squared electric field in Fig. 8(a) does not represent an intersection of the branches in the full solution space. In the plot of squared electric field, one continuous branch of solutions rises to a maximum, then decreases to zero in a reversed s-shaped curve. This branch is mutlivalued in frequency also. The other rises monotonically from zero, starting at a higher excitation parameter value than the first. The crossover point

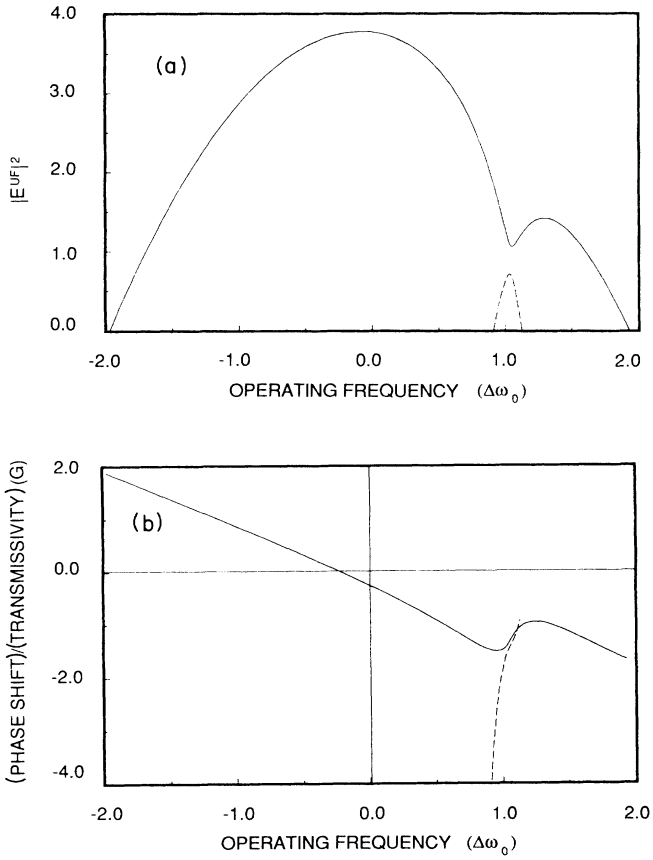

FIG. 6. Squared electric field vs operating frequency $\Delta\omega_0$ (a) and the phase-shift—transmissivity ratio vs operating frequency (b) for $\Delta\omega_{ab}=\gamma_{\perp a}$ (that is, the absorber line-center frequency ω_b is higher than that of the amplifier, ω_a, by $\gamma_{\perp a}=100\times10^6$ sec^{-1}). The excitation parameter value for these plots is $A=4.90I_{sa}$. These plots are analogous to those of Figs. 2 and 3, where $\Delta\omega_{ab}=0$. In the present case, the overall asymmetry in the solution for squared electric field causes the dip in the primary solution and the peak of the secondary solution to be asymmetric; furthermore, the extrema occur at different values of $\Delta\omega_0$, neither of which equals $\gamma_{\perp a}$.

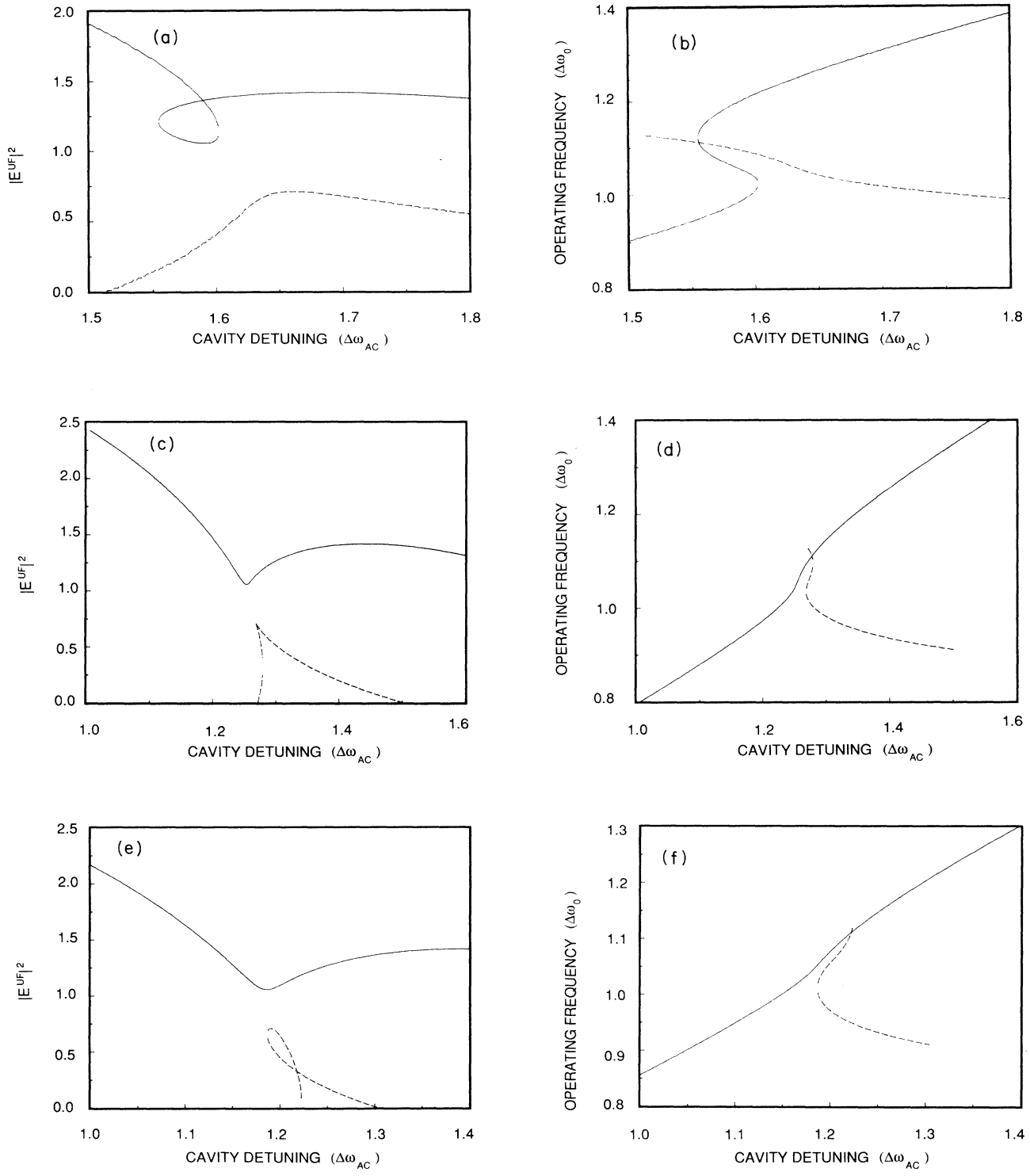

FIG. 7. Squared electric field (a), (c), and (e) and operating frequency $\Delta\omega_0$ (b), (d), and (f) vs detuning for $\Delta\omega_{ab}=\gamma_{\perp a}$ and $A=4.90I_{sa}$, corresponding to Fig. 6. Cavity linewidths are (a) and (b), $\kappa=0.40\gamma_{\perp a}$; (c) and (d), $\kappa=0.125\gamma_{\perp a}$; and (e) and (f), $\kappa=0.065\gamma_{\perp a}$, where $\gamma_{\perp a}=100\times10^6$ sec^{-1} in all cases. Solid curves represent primary solutions and dashed curves, secondary solutions. These curves are topologically like those of Fig. 4, but are asymmetric due to the offset in the line-center frequencies of the amplifying and absorbing media. Because of this, the degree of mutlivaluedness of some of these plots is different from that of the corresponding plots in Fig. 4.

occurs at a higher excitation value than the maximum of the first branch, at a junction of two single-value segments of the first branch. If one were to increase the excitation from zero, the system would be expected to follow the first branch, then hop to the second; but as excitation is decreased from some high value, it is not clear whether or where the system would hop from the second branch back to the first. It is even conceivable that it could follow the second branch all the way to zero intensity, and then hop up to the first. Any such jumps in intensity would also be accompanied by jumps in frequency. The stability analysis will help resolve these questions.

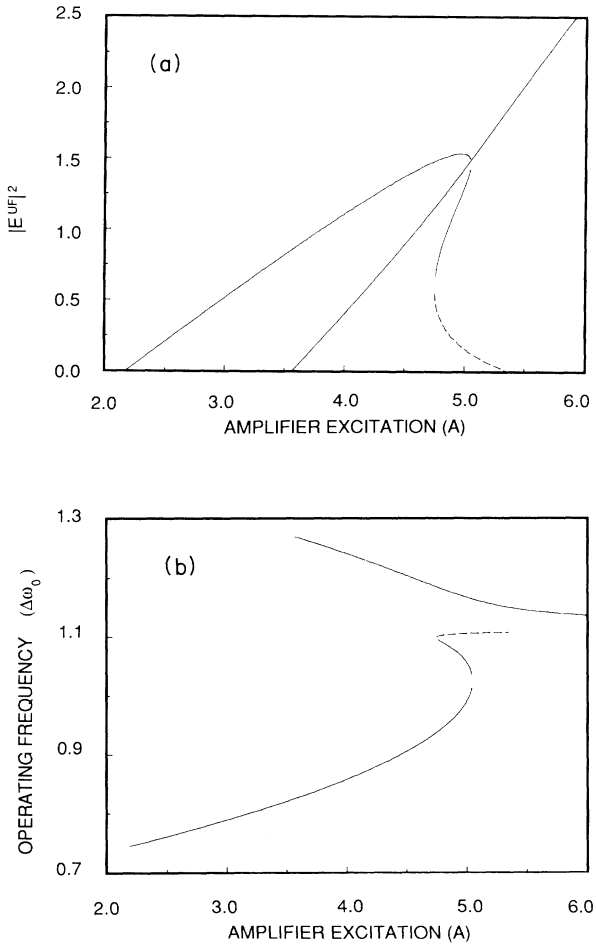

FIG. 8. Squared electric field (a) and operating frequency $\Delta\omega_0$ (b) vs amplifying medium excitation parameter for $\Delta\omega_{ab}=\gamma_{\perp a}$. The cavity linewidth $\kappa=0.40\gamma_{\perp a}$ and the cavity detuning $\Delta\omega_{ac}=1.57\gamma_{\perp a}$. Solid curves are primary solutions; dashed curves are secondary solutions. Sections through the plots at $A=4.90I_{sa}$ correspond to sections through the plots of Figs. 7(a) and 7(b) at a cavity-detuning value of $\Delta\omega_{ac}=1.57\gamma_{\perp a}$. The plots shown here may be compared to the plots of Figs. 5(a) and 5(b), for which $\Delta\omega_{ab}=0$. Here the monotonic branch of solutions has shifted to higher excitation parameter values, relative to the multivalued branch. This may give rise to more complicated bistability and hysteresis behavior than occurs in the case of $\Delta\omega_{ab}=0$. See the text for further discussion.

A comparison of Fig. 8 with Figs. 5(a) and 5(b) suggests that one can roughly picture the effects of cavity detuning and the separation of amplifier and absorber line-center frequencies on these plots as a relative horizontal sliding of the monotonic and nonmonotonic branches of solutions. The figures indicate that these effects may work in opposite directions. One concludes that some combination of line-center separation and nonzero detuning will cause the points where these branches bifurcate from zero intensity to coincide, as they do in the fully tuned case. Unlike the fully tuned case, there would not be whole regions of degeneracy.

This case is the first presented here in which the solution of maximum intensity exists first on one continuous branch of solutions, and then on another, as a control parameter varies. However, this may not be particularly significant, in that all multivalued branches of solutions may be considered to be composed of shorter single-valued branches. Then hysteresis in any case is expected to involve a jump from one single-valued branch to another, and the fact that some branches link end to end in solution space may not have any bearing on the dynamics of the system. Again, a stability analysis will be helpful.

VII. SUMMARY AND CONCLUSION

We have presented a method of obtaining steady-state solutions incorporating depndences on detuning, excitation, and atomic line-center frequencies for a semiclassical model of the ring laser with a saturable absorber. We believe this is the first theoretical work to study these properties of the system in such detail. The results obtained show how cavity detuning, laser excitation, cavity linewidth, and the line-center frequencies of the media interact to determine the possible steady-state solutions. Results of this type were found for the limiting case of uniform electric field amplitude [the uniform-field approximation, often called the mean-field approximation, Ref. 7(a)]. However, the solutions found also allow numerical calculations of the longitudinal position dependence of the steady-state electric field amplitude, as well as that of the other state variables. The formulation of such a calculation for this system is also a new result. A summary of the model, the methods, and the main results and predictions follows.

We began with a model which assumed that the amplifying and absorbing media were mixed in the same cell, and that each medium consisted of homogeneously broadened two-level atoms. The system was modeled mathematically by the semiclassical Maxwell-bloch equations, assuming single-frequency solutions in the slowly varying amplitude approximation. Light was assumed to propagate unidirectionally around the cavity. Polarization of the light and variations of the electric field and other variables transversely to the optical axis were ignored.

The spatially dependent steady-state solutions of the Maxwell-Bloch equations were obtained with the help of a transformation which converts the equations and their boundary condition into a set of purely real equations. In

order to simplify these results and compare them with the findings of others, the uniform-field approximation was applied to them. The results of this procedure gave "state space" plots of squared electric field amplitude versus operating frequency and of the phase-shift—transmissivity ratio versus operating frequency. Over various ranges of operating frequency, zero, one, or two steady-state solutions were found. How many solutions there are and over what ranges of operating frequency they exist was found to depend upon the degree of excitation of each medium.

These results were combined with the boundary condition to give squared electric field amplitude and operating frequency versus various control parameters—in particular, cavity detuning and laser excitation. This step was considered from the viewpoint of a graphical method developed by Casperson and Yariv, which provided physical insight into the mathematical procedures and suggested the method of numerical solution employed.

In general each of the two possible state-space solutions gave rise to as many as three roots when the steady states were found as functions of cavity detuning or laser excitation. However, it was observed that there were no more than four physically significant roots in total for any combination of parameter values. The number and behavior of the roots given by each state-space solution was found to depend strongly on the cavity linewidth. For example, with fixed laser excitation and variable detuning, each of the two state-space solutions gave a branch of solutions on a detuning plot. The cavity linewidth and the difference between the line-center frequencies of the absorbing and amplifying media determined which branch, if either, was multivalued.

Plots of squared electric field and of operating frequency versus laser excitation for the fully tuned case were found to agree with results previously obtained by others. In particular, there were two branches of steady-state solutions giving different operating frequencies but the same values for squared electric field at a given excitation, and two other branches having different values for squared electric field but the same values for operating frequency. All four branches met at a common point, whose position varied with the cavity linewidth. This dependence of the plots on cavity linewidth also agreed with the previous findings. The presence of cavity detuning or of differing line-center frequencies for the media broke the degeneracies and eliminated the common point of intersection. Instead, there were two continuous branches of solutions, one of which bifurcated from the zero-field solution at a lower value of laser excitation than the other. This suggested that increasing laser excitation from zero in the presence of detuning would lead to the appearance of a steady-state solution rather than the small-amplitude pulsing found in the fully tuned case. Since the breaking of degeneracy occurs for any small detuning, it was concluded that an actual laser would behave in the manner described here, because mathematically exact tuning cannot be achieved in practice. When the two media had a common line-center frequency, the branch of solutions bifurcating from zero at lower excitation always had a greater amplitude than the other branch; the latter eventually returned to zero field. If the line-center frequencies of the two media were sufficiently different, the branch which eventually returned to zero field bifurcated from zero at a lower value of excitation than the other branch. In such a case, first one branch and then the other has the higher value of electric field amplitude. This reversal raises interesting questions about the stability of the two branches and the occurrence of hysteresis and bistability in such cases.

Questions such as these can be answered, at least in part, with the help of a linearized stability analysis of the steady-state solutions. Such an analysis is presently underway and will be reported separately.

ACKNOWLEDGMENTS

The authors wish to express their gratitude to the staff of the Bryn Mawr College Office of Academic Computing Services for assistance with the numerical computations, especially J. M. Anderson, J. A. Malsbury, and A. Gunn. We are grateful to Professor Paul Mandel for helpful conversations and generous encouragement. N.B.A. and D.E.C. initially discussed this problem while visting the Mathematics Department of the University of Calabria (Arcavacata di Rende, Cosenza, Italy), and wish to thank the Department and Professor M. Martelli for their hospitality at that time. N.B.A. and A.M.A. have been supported in part by National Science Foundation Grant No. EC-8210263 during the course of this work. D.E.C. was supported in part by Bryn Mawr College. This work is submitted to the faculty of Bryn Mawr College in partial fulfillment of the requirements of the Ph.D. degree for David E. Chyba.

---

*Present address: Physik-Institut der Universität Zürich, Schönberggasse 9, CH-8001 Zürich, Switzerland.

[1](a) L. A. Lugiato, P. Mandel, S. T. Dembinski, and A. Kossakowski, Phys. Rev. A **18**, 238 (1978); (b) S. T. Dembinski, A. Kossakowski, L. A. Lugiato, and P. Mandel, *ibid.* **18**, 1145 (1978); (c) S. T. Dembinski, A. Kossakowski, P. Peplowski, L. A. Lugiato, and P. Mandel, Phys. Lett. **68A**, 20 (1978).

[2](a) P. Mandel, Phys. Rev. A **21**, 2020 (1980); (b) Phys. Lett. **83A**, 207 (1981); (c) T. Erneux and P. Mandel, Z. Phys. B **44**, 353 (1981); (d) **44**, 365 (1981); (e) T. Erneux, P. Mandel, and J. F. Magnan, Phys. Rev. A **29**, 2690 (1984); (f) P. Mandel and T. Erneux, *ibid.* **30**, 1893 (1984); (g) T. Erneux and P. Mandel, *ibid.* **30**, 1902 (1984); (h) T. Erneux, in *Optical Instabilities*, edited by R. W. Boyd, M. G. Raymer, and L. M. Narducci (Cambridge University Press, Cambridge, 1986), pp. 99—110.

[3](a) F. Mrugala and P. Peplowski, Z. Phys. B **38**, 359 (1980); (b) P. Peplowski, Physica **6D**, 364 (1983).

[4](a) J. C. Antoranz and M. G. Velarde, Opt. Commun. **38**, 61 (1981); (b) J. C. Antoranz, J. Gea, and M. G. Velarde, Phys. Rev. Lett. **47**, 1895 (1981); (c) J. C. Antoranz, L. L. Bonilla, J.

Gea, and M. G. Velarde, Phys. Rev. Lett. **49**, 35 (1982); (d) M. G. Velarde, in *Evolution of Order and Chaos,* edited by H. Haken (Springer-Verlag, New York, 1982), pp. 132–145; (e) M. G. Velarde and J.C. Antoranz, in *Optical Instabilities,* edited by R. W. Boyd, M. G. Raymer, and L. M. Narducci (Cambridge University Press, Cambridge, 1986), pp. 287–292.

[5]X.-G. Wu and P. Mandel, J. Opt. Soc. Am. B 3, 724 (1986).

[6]A method similar to ours has been used to find the longitudinal dependence of the electric field amplitude in a homogeneously broadened ring laser by L. A. Lugiato, L. M. Narducci, E. V. Eschenazi, D. K. Bandy, and N. B. Abraham, Phys. Rev. A **32**, 1563 (1985).

[7](a) R. Bonifacio and L. A. Lugiato, Lett. Nuovo Cimento **21**, 505 (1978). We refer to their mean-field approximation as the uniform-field approximation to avoid confusion with the mean-field approximation technique of statistical mechanics. This change in the traditional terminology of optical bistability and laser physics is made in conformity with the usage suggested by the review cited in Ref. 16; (b) V. Benza and L. A. Lugiato, Z. Phys. B **35**, 383 (1979); (c) M. Gronchi and L. A. Lugiato, Opt. Lett. **5**, 108 (1980).

[8]E. Arimondo and B. M. Dinelli, Opt. Commun. **44**, 277 (1983).

[9](a) R. Salomaa and S. Stenholm, Phys. Rev. A **8**, 2695 (1973); (b) **8**, 2711 (1973).

[10]V. S. Letokhov and V. P. Chebotaev, Usp. Fiz. Nauk. **113**, 385 (1974) [Sov. Phys.—Usp. **17**, 467 (1975)], and references cited therein.

[11]R. Müller, Opt. Commun. **33**, 326 (1980).

[12]A. G. Kagan and Ya. I. Khanin, Kvantovaya Elektron. (Moscow) **10**, 149 (1983) [Sov. J. Quantum Electron. **13**, 88 (1983)], and references cited therein.

[13](a) E. Arimondo, F. Casagrande, L. A. Lugiato, and P. Glorieux, Appl. Phys. B **30**, 57 (1983); (b) M. L. Asquini and F. Casagrande, Nuovo Cimento **2D**, 917 (1983).

[14]J. C. Englund and W. C. Schieve, J. Opt. Soc. Am. B 2, 81 (1985).

[15]H. Atmanspacher, H. Scheingraber, and C. R. Vidal, Phys. Rev. A **32**, 254 (1985), and references cited therein.

[16]N. B. Abraham, P. Mandel, and L. M. Narducci, Prog. Opt. (to be published).

[17]V. S. Letokhov and V. P. Chebotayev, *Nonlinear Laser Spectroscopy* (Springer-Verlag, New York, 1977).

[18](a) V. N. Lisitsyn and V. P. Chebotaev, Zh. Eksp. Teor. Fiz. **54**, 419 (1968) [Sov. Phys.—JETP **27**, 227 (1968)]; (b) M. Gronchi and A. Sona, Riv. Nuovo Cimento **2**, 219 (1970); (c) J. B. Cole, J. Phys. D **8**, 1392 (1975).

[19](a) V. P. Chebotayev, I. M. Beterov, and V. N. Lisitsyn, IEEE J. Quantum Electron. **QE-4**, 788 (1968); (b) P. W. Smith, Proc. IEEE **58**, 1342 (1970); (c) A. J. Demaria, in *Progress in Optics,* edited by E. Wolf (North-Holland, Amsterdam, 1971), Vol. IX, pp. 31–71; (d) J.-C. Diels, W. Dietel, J. J. Fontaine, W. Rudolph, and B. Wilhelmi, J. Opt. Soc. Am. B 2, 680 (1985), and references cited therein; (e) N. M. Lawandy and D. L. MacFarlane, in *Optical Instabilities,* edited by R. W. Boyd, M. G. Raymer, and L. M. Narducci (Cambridge University Press, Cambridge, 1986), pp. 284–286, and references cited therein.

[20](a) E. Arimondo and P. Glorieux, Appl. Phys. Lett. **33**, 49 (1978); (b) A. Jacques and P. Glorieux, Opt. Commun. **40**, 455 (1982); (c) E. Arimondo, P. Bootz, P. Glorieux, and E. Menchi, J. Opt. Soc. Am. B 2, 193 (1985); (d) E. Arimondo and E. Menchi, Appl. Phys. B **37**, 55 (1985); (e) P. Glorieux and D. Dangoisse, IEEE J. Quantum Electron. **QE-21**, 1486 (1985); (f) E. Arimondo, C. Gabbanini, E. Menchi, D. Dangoisse, and P. Glorieux, in *Optical Instabilities,* edited by R. W. Boyd, M. G. Raymer, and L. M. Narducci (Cambridge University Press, Cambridge 1986), pp. 277–280.

[21](a) R. Ruschin and S. H. Bauer, Chem. Phys. Lett. **66**, 100 (1979); (b) R. Ruschin and S. H. Bauer, Appl. Phys. **24**, 45 (1981).

[22]J. Heppner, Z. Solajic, and G. Merkle, Appl. Phys. B **35**, 77 (1984).

[23]L. W. Casperson and A. Yariv, Appl. Phys. Lett. **17**, 259 (1970).

[24]The boundary condition can be understood by considering the full expression for the space and time dependence of the electric field at position z and time t in the slowly varying amplitude approximation, $E(z,t)\exp[i(k_0 z-\omega_0 t)]$. Here k_0 denotes the wave number in free space. At $z=0$, this expression reduces to $E(0,t)\exp(-i\omega_0 t)$. But a feature of the wave field appearing at $z=0$ at time t was at position $z=L$ at a time Δt earlier. At that place and time, the field amplitude was larger by $1/R$, due to the cavity losses. Therefore we may write

$$(1/R)E(0,t)\exp(-i\omega_0 t) = E(L,t-\Delta t)\exp(ik_0 L)\exp[-i\omega_0(t-\Delta t)] .$$

The boundary condition then follows if we put $k_0=\omega_0/c$, $(\Delta t+L/c)=t_R$, and use $\exp(i\omega_0 t_R)=\exp(-i\Delta\omega_c t_R)$. This last equality holds because $\exp(-i\omega_c t_R)\equiv 1$. It is worth noting that the boundary condition by itself describes nothing more than the propagation of the wave field from one point to another with a proportionate loss. Together with the Maxwell-Bloch equations, it relates the input to the medium cell at time t to the output of the cell at time $t-\Delta t$. In the steady state, this implies phase and amplitude matching of the wave field with itself after a trip around the cavity. The t dependence in the boundary condition also allows for a time evolution in which the amplitude and phase at a given position need not be the same on successive traversals of the field around the cavity. This is consistent with the physical picture of a running wave circulating around the cavity unidirectionally and evolving in time through interaction with the medium. However, any time evolution must be slow compared to t_R to be consistent with the assumption of a single-frequency solution in the slowly varying amplitude approximation.

[25](a) D. E. Chyba, N. B. Abraham, and A. M. Albano (unpublished); D. E. Chyba, Ph.D. dissertation, Bryn Mawr College, 1986 (unpublished).

[26]Formally, one can also use the mode-line analysis in solving Eqs. (2.14). However, the method is not so useful in this situation, because changes in various parameters affect both sides of Eq. (2.14b). Without the uniform-field approximation, the mode line does not behave independently of the right side of the equation.

[27]W. L. Faust and R. A. McFarlane, J. Appl. Phys. **35**, 2010 (1964).